Category representations in the primary visual cortex support orientation discrimination

Julien Corbo[1], O. Batuhan Erkat[1,2], John McClure Jr.[1,2], Hussein Khdour[1,2], & Pierre-Olivier Polack[1]✉

bioRχiv
THE PREPRINT SERVER FOR BIOLOGY

Perceptual discrimination requires the ability to determine that two stimuli are different. It is well established that neuronal representations in sensory cortices (i.e. the specific neuronal activity patterns evoked by the stimuli) are essential for perceptual choice [1–4]. Yet, the general principles by which those representations are compared in sensory systems remain paradoxically elusive. Indeed, the resolution of the neuronal representations is an order of magnitude more precise than the discrimination capabilities of the animals during behavioral tasks [5–9]. This large discrepancy between theoretical neural resolution and actual animal discrimination threshold suggests that the integrative mechanisms leading to perceptual decision are computationally limited. To determine those computational constraints, we recorded the activity of layer 2/3 neurons in the primary visual cortex (V1) of mice performing a Go/NoGo orientation discrimination task. We found that two oriented cues were perfectly perceived as distinct when there was no overlap between their neuronal representations. However, at the limit of discriminability, V1 activity stopped encoding for the orientation of the visual stimulus. Instead, we observed a funneling of the V1 activity toward distinct domains of the orientation representation space, likely generated by an orientation-dependent modulation of the neuronal excitability. The relative neuronal activity at those domains provided a probabilistic indication that the stimulus belonged to the Go or NoGo category. Thus, the categorical classification by V1 of the presented stimulus predicts accurately the probabilities of the animals' perceptual decisions.

Perception results from the detection and interpretation by the central nervous system of the information provided by the sensory organs. Perception is delimited positively by a threshold above which a stimulus can be detected (detection threshold), and a limit above which two different stimuli can be discriminated (limit of resolution or resolving power). While the detection threshold is constrained by the signal-to-noise ratio of the encoded stimulus [10], the resolution is determined by the limit below which the neuronal activity patterns representing the two stimuli cannot be distinguished [11,12]. Hence, understanding the constraints limiting the resolving power can provide an essential indication on the link existing between sensory processing and sensory perceptions. Currently, our models fail at predicting perceptual behavior from the neuronal activity [12]. Indeed, models based on selective pooling [8,13–17], or weight pooling [18–20] outperform the discrimination capability of the animals [5–9]. Thus, a simple linear decoder using the neuronal activity of the primary visual cortex (V1) can distinguish orientations less than a degree apart [9], when mice cannot discriminate between orientations separated by an angle smaller than 20° [21,22]. Yet, it is well established that V1 is the cortical territory encoding oriented stimuli [23–25], and is necessary for resolving orientation discrimination tasks [2–4,6,26–28].

Perceptual discrimination and neuronal representation similarity

This discrepancy of several orders of magnitude between psychometric and neurometric curves suggests that perceptual discrimination does not result from the approaches of neuronal information selection and integration typically tested [9]. Therefore, we tested the hypothesis that two stimuli are perceived as different if their cortical representations (i.e., the neuronal population activated by the stimulus) do not overlap [11,12]. To determine the minimal overlap of neuronal representation necessary for orientation discrimination, we trained 10 mice to perform a Go/NoGo task that consisted in licking in response to a Go visual cue (a 45° drifting grating) and withhold licking during the third second of the presentation of the NoGo cue (a 135° drifting grating; Fig. 1a). Once mice reached an optimal performance using orthogonal cues (Fig. 1b), we assessed the mouse orientation discrimination abilities in six consecutive daily recording sessions during which the angle between the orientations of the Go and NoGo cues was progressively reduced (Go/NoGo angle decreasing from 90° to 15°; Fig. 1a,b; see Methods). Below 30°, the mice performance steadily decreased, driven by an increase in the false alarm (FA) rate. When the Go/NoGo angle was 15°, the mouse D' was systematically under the best random D' value (brD' = 1.7; see Methods) suggesting that the mice choice was not based on perceptual discrimination (Fig. 1b), and that the discrimination threshold was between 30° and 15°, a value similar to the orientation discrimination thresholds described in studies using similar tasks in rodents [21,22]. During each session, we imaged the activity of V1 L2/3 cortical neurons as orientation discrimination tasks were previously shown to rely on V1 neuronal activity [26–28]. The fractional fluorescence (ΔF/F) was deconvolved in Action Potential related Events [29,30] (APrEs; Fig. 1c,d). Then, we assessed the similarity between the patterns evoked by the Go and NoGo cues (Fig. 1e) by measuring their cosine similarity (Fig. 1f,g). When plotting the mouse performance as a function of the similarity between the Go and NoGo population response patterns (Fig. 1h), we found a negative correlation between animal performance and V1 population response similarity (sigmoid fit: $r^2 = 0.38$; inflection point: similarity = 0.70±0.1) confirming that an excessive similarity between the Go and NoGo population responses is detrimental for the behavioral performance.

Categorical domains in the orientation space

To determine how this response similarity was structured in the orientation space, we sorted the activity of V1 neurons by their preferred orientation[29] (Fig. 2a; see Method). The tuning blocks (series of 12 different drifting gratings), used to assess the neurons' preferred orientations, were typically performed at the end of the recording sessions (Fig. 1a). However, presenting the tuning block at the beginning or at the end of the session led to a similar measure of the neurons' orientation preference (Extended Data Fig. 1a-c). When the Go/NoGo angle was greater or equal to 45°, the representations of the Go and the NoGo cues in the orientation space were completely distinct (Fig. 2a,b; Extended Data Fig. 2). For a Go/NoGo angle ranging from

1. Center for Molecular and Behavioral Neuroscience. Rutgers University – Newark, USA.2. Behavioral and Neural Sciences Graduate Program, Rutgers University – Newark,USA. ✉ e-mail: polack.po@rutgers.edu

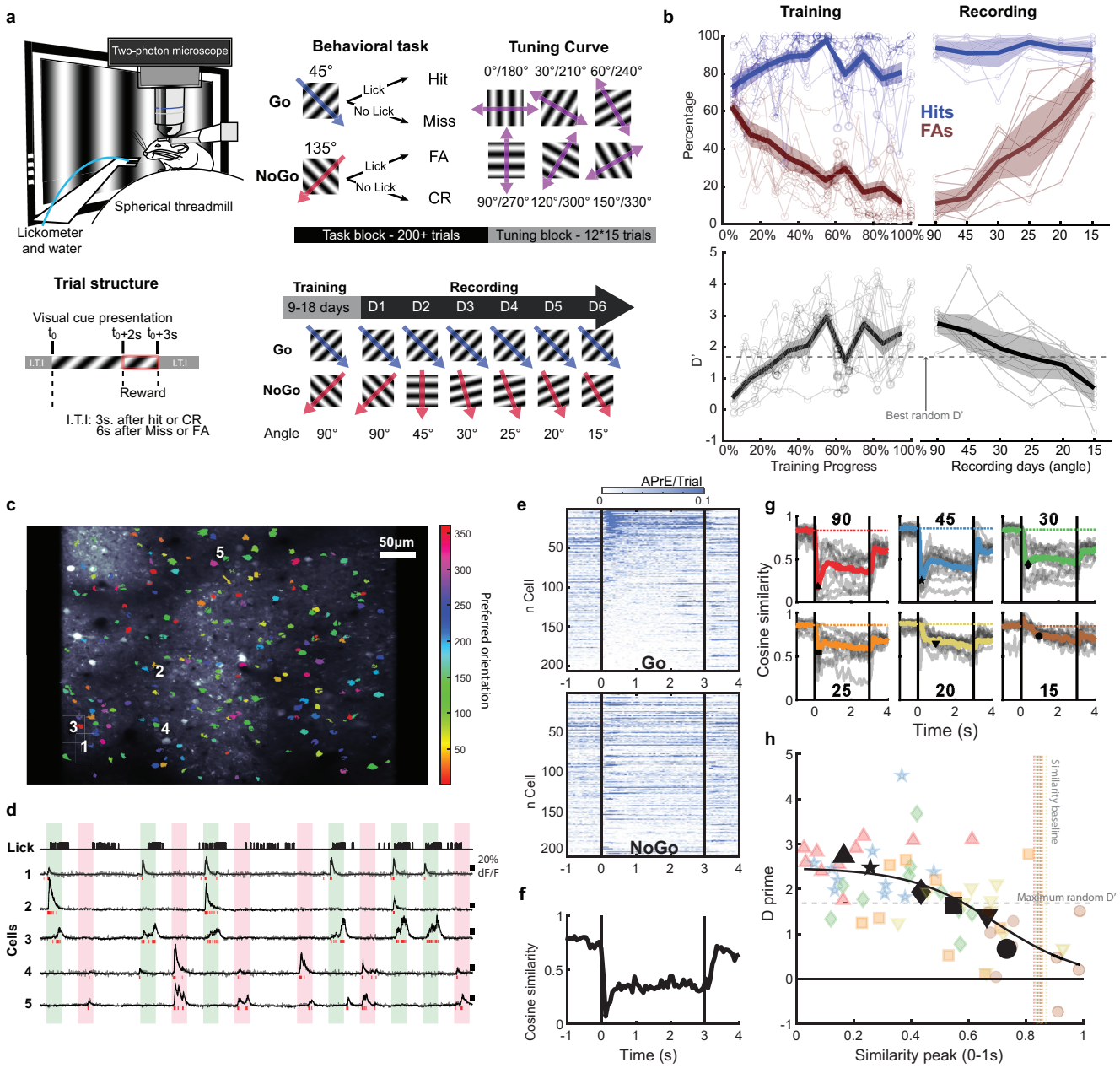

Fig. 1 | Neuronal response similarity in the V1 of mice performing an orientation discrimination task. a. Schematic representation of the experimental setup, including the trial temporal structure (bottom left panel), the session organization (top right panel), and the Go and NoGo stimuli used for the different recording sessions (bottom right panel) **b.** Mice behavioral performance during training and recording sessions. Top panels: chance of hit trials during the presentation of the Go cue (blue), and of false alarms (FAs) during the presentation of the NoGo cue (red). **c.** Two-photon calcium image of recorded neurons on which are overlapped the neurons' preferred orientations. **d.** Fractional fluorescence (ΔF/F, bottom traces) of the five neurons indicated in (c.) during the orientation discrimination task. Neurons 1-3 are tuned to the Go orientation. Neurons 4 and 5 are tuned to the NoGo orientation. Top trace: mouse licking activity. Short red lines indicate time of action potential related events (APrEs). **e.** Mean APrE activity of 206 simultaneously recorded neurons during the presentation of the Go (top panel) and NoGo cues (bottom panel). Neurons are ordered as a function of their response intensity to the Go stimulus presentation. **f.** Cosine similarity between the neuronal activity patterns shown in (e). **g.** Same representation as in (f) for all the Go/NoGo angles of all the mice (colored lines indicate averages across mice). **h.** Mouse performance (D') as a function of the cosine similarity between the Go and NoGo responses during the first second of the visual stimulus presentation. Color code for individual session correspond to the one indicated in (g). Black shapes indicate the mean across mice for the same Go/NoGo angle. Vertical colored lines indicate the similarity measured during the baseline activity immediately the visual stimulus. The horizontal line indicates the maximum D' that can be obtained with random performance.

30° to 20° (i.e., at the limit of the behavioral discrimination threshold), the overlap in the orientation space between the responses evoked by the Go and NoGo cues started to increase when the Go/NoGo angle decreased (Fig.2c-f; Extended Data Fig. 2). Concurrently, the V1 responses evoked by NoGo cues in the orientation space stopped being a unimodal distribution centered around the orientation of the presented stimulus (Fig.2c,d; Extended Data Fig. 2). Instead, the NoGo cue representation was bimodal with a peak around 45° (i.e., the orientation of the Go visual stimulus) and another that remained around 90° regardless of the orientation of the NoGo stimulus. When the Go/NoGo angle decreased, the activity in the orientation space surrounding 45° increased while the activity surrounding 90° decreased (Extended Data Fig. 2). The bimodality of the NoGo stimulus representation in the orientation space disappeared when the Go/NoGo angle was 15° (Fig.2e,f). To determine the variability of this distribution of activity in the orientation space across trials, we determined for all Go/NoGo angles the location of the peak of activity in 1000 resampled trials (Fig.2g). This analysis confirmed that for Go/NoGo an-

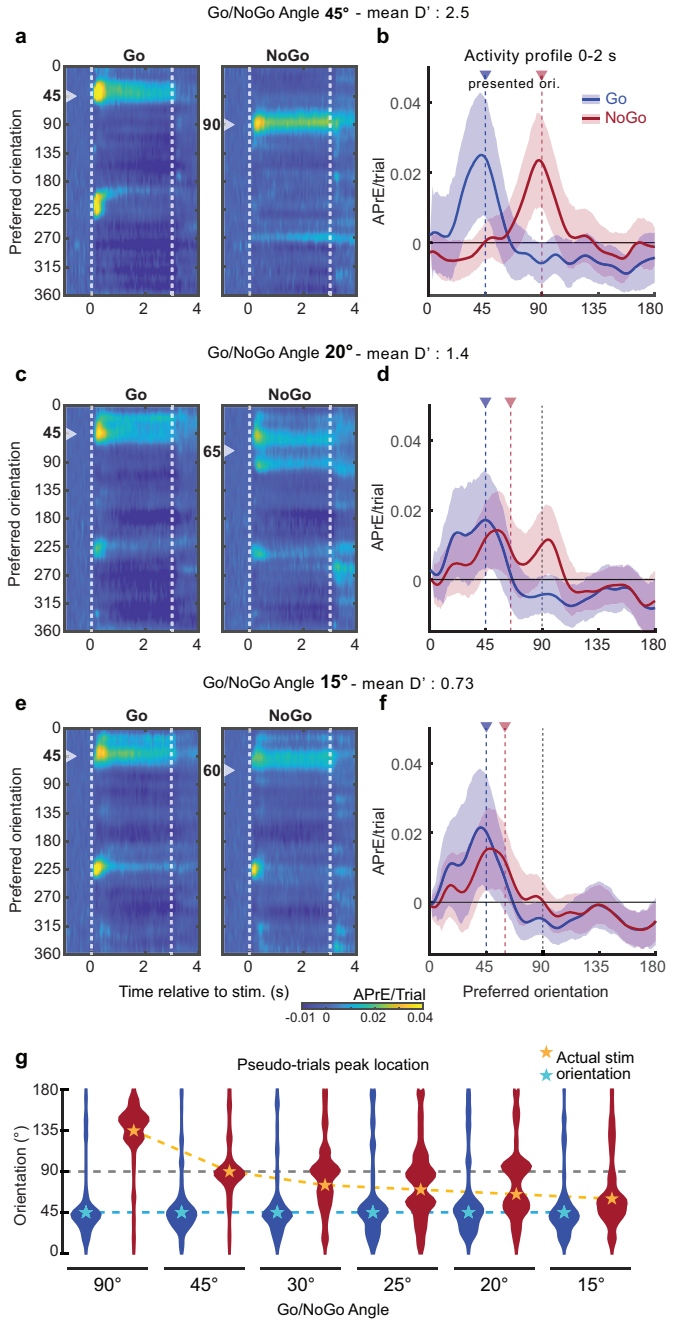

Fig. 2 | Go and NoGo stimulus representations in the orientation space as a function of the Go/NoGo angle. a. Neuronal activity evoked by the Go (left panel) and NoGo stimuli (right panel) as a function of V1 neurons' preferred orientations when the Go/NoGo angle is 45°. Neuronal activity color scale is located at the bottom of the panel (c). The mean behavioral performance (D') across mice is indicated on top. **b.** Mean activity evoked in the orientation space by the Go (45°, blue) and NoGo (90°, red) stimuli during the two first seconds of the stimulus presentation. Vertical colored lines indicate the orientation of the presented stimulus. Shaded areas indicate the s.e.m. **c.** Same representation as in (a) when the angle between the Go/NoGo angle is 20°. **d.** Same representation as in (b) when the NoGo orientation is 65°. **e.** Same representation as in (a) when the Go/NoGo angle is 15°. **f.** Same representation as in (b) when the NoGo orientation is 60°. **g.** Violon plot of the peak of activity in the orientation space during the Go (blue) and NoGo (red) pseudo-trials. Blue and gold stars indicate the orientation of the Go and NoGo stimuli respectively.

gles ranging from 30° to 20°, the distribution of the peaks of activity during the presentation of the NoGo cue was bimodal and that those peaks did not correspond to the orientation of the presented stimulus. Hence, between 45° to 20° Go/NoGo angles, the neuronal activity evoked by the Go and NoGo cues activated two 'domains' of the orientation space: the Go domain (around 45°) and the NoGo domain (around 90°). We further confirmed that this bimodal representation was not due to averaging the activity across trials and across similarly tuned neurons (Extended Data Fig. 3a) as the coactivation of the Go and NoGo domains could be found at the trial level in single sessions when the Go/NoGo angle was between 30° and 20° (Extended Data Fig. 3b). Those results suggested the existence of a relationship between the distortion of the orientation space [29], characterized by the presence of the Go and NoGo domains, and the limit of perceptual discrimination.

To evidence the relationship between the bimodal representation of the NoGo cue and behavioral performance, we needed a manipulation that could modulate the animal behavioral performance for the same stimuli and the same task. We know that adding sounds to the presentation of an oriented visual stimulus improves orientation discrimination in humans [31,32] but also can modify orientation representations in mouse V1 [33,34]. Therefore, a second experimenter trained a new set of mice, but this time the recording sessions were made of two blocks: a unimodal block where mice performed in the same condition as the first set of mice, and an audiovisual block during which the same visual stimuli were randomly paired with either a high pitch (10 kHz) or a low pitch (5 kHz) tone. We found that sounds improved the mouse orientation discrimination performance in the same session (Fig. 3b). This perceptual improvement was driven by the decrease of the FA rate (Fig. 3c; Extended Data Fig. 4). The maximal improvement was found when the Go/NoGo angle was 25° (Fig. 3c), i.e., around the best random D' value (beD' = 1.0; Fig. 3b). To determine if this behavioral improvement was associated with a modification of the activation of the Go and NoGo domains in V1, we compared the Go and NoGo cue representations in the orientation space between the unimodal and audiovisual contexts (Fig. 3d; Extended Data Fig. 4). The results reproduced our initial findings: for wide Go/NoGo angles and below the orientation discrimination threshold (i.e., Go/NoGo angles ≥45° or ≤20°), the Go and NoGo cues were represented by a unimodal distribution in the orientation space centered on the orientation of the presented stimulus. However, in the vicinity of the discrimination threshold (~ 25°), the representation of the NoGo cue was bimodal with a peak of activity around the orientation of the Go cue and another around 90° which did not correspond to the orientation of the NoGo stimulus (Fig. 3d,e; Extended Data Fig. 4). Remarkably, when comparing the representation of the NoGo orientation in the unimodal and audiovisual contexts, we found that the largest peak of activity in the unimodal context (mean D' ± s.e.m. = 0.8 ± 0.2; poor performance) was for the neurons of the Go domain (45°). While, in the audiovisual context (D' = 1.5 ± 0.1; improved performance), the largest peak of activity was carried by neurons tuned for the NoGo domain (Fig. 3d,e; Extended Data Fig. 4). Altogether our results demonstrated in two independent datasets generated by two different experimenters that, around the behavioral discrimination threshold, the NoGo stimulus is represented in orientation space by two neuronal populations: a population tuned for orientations surrounding the orientation of the Go stimulus (the Go domain), and another population tuned for orientation surrounding 90° (the NoGo domain). This NoGo domain orientation does not correspond to the orientation of the NoGo stimulus and remains similar across Go/NoGo angles flanking the behavioral threshold and across datasets.

Categorical representation explains perceptual decision

The results obtained with the audiovisual dataset suggested that the relative activation by the NoGo visual stimulus of the two neuronal populations (the neurons of the Go domain: preferred orientation: 1° - 60°, and the neurons of the NoGo domain: preferred orientation: 61° - 120°) was linked to the animal behavioral performance. To test this hypothesis, we defined the Go evidence as the ratio of the APrE activity in the Go domain and the sum of APrE activity in the Go and NoGo domains (Fig. 4a). Then, for each Go/NoGo angle of the two datasets, we plotted the mouse licking probability as a function of the Go evidence for every time point of the visual stimulus presentation. The linear fit between Go evidence and mouse task performance explained more than 80% of the behavioral variance within 250 milliseconds of the stimulus presentation (Fig. 4b,c). The variance explained by the Go evidence was significantly greater than the variance explained by the Go domain activity or the NoGo domain activity alone (Fig. 4c) suggesting that neuronal activities of both domains were important for the animal's decision. As our results were obtained from averaging the neuronal activity of successful and unsuccessful trials, it was possible that the relative activation of the two domains could predict the performance of the animal at the trial level. We therefore tested the hypothesis that FA could be triggered during the presentation of the

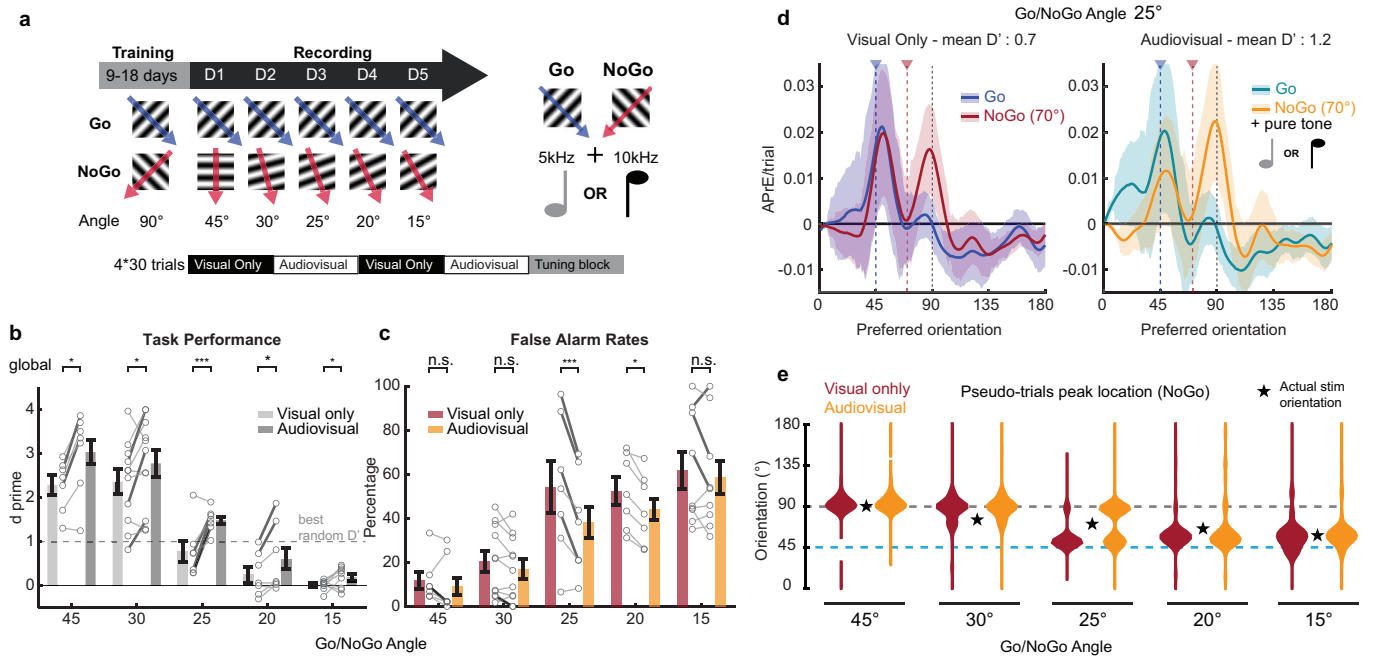

Fig. 3 | Orientation representation and the behavioral performance in unimodal and audiovisual contexts. a. Go and NoGo stimuli used during the training and recording sessions (top left panel). Sessions alternated unimodal and audiovisual blocks and ended with a tuning block (bottom panel). During audiovisual blocks Go and NoGo cues were paired with either a 5 kHz or a 10 kHz tone. **b.** Behavioral performance during the unimodal visual (light grey) and audiovisual (dark grey) blocks of the different recording session. Black lines indicate mean ± s.e.m. across sessions. Permutation test: *: p<0.05; ***: p<0.001. White dots indicate individual mice (thick lines indicate significant difference; p<0.05). **c.** Same representation as in (b) for the FA rate. **d.** Left panel: mean activity evoked in the orientation space by the Go (45°, blue) and NoGo (70°, red) cues during the two first seconds of the unimodal visual stimulus presentation. Right panel: mean activity evoked in the orientation space by the same Go (45°, green) and NoGo (70°, yellow) stimuli during the same period. Vertical colored lines indicate the orientation of the presented stimulus. Shaded areas indicate the s.e.m. **e.** Violin plot of the distribution of the location in the orientation space of the peak of activity for unimodal NoGo (red) and audiovisual NoGo (yellow) pseudo-trials. Gold stars indicate the orientation of the presented NoGo stimulus.

NoGo cues because of an excess of Go evidence. To do so, we separated the average activity profiles evoked during FA and correct rejection (CR) trials and found that they overlapped in the orientation space (Extended Data Fig. 5a). This invariance of the representations across animal decisions was also found at the trial level (Extended Data Fig. 5b). Indeed, plotting the activity in the Go and NoGo domain against each other showed that single trial activity did not move systematically in the direction of more Go evidence when the animal licked compared to when they withhold licking. (Extended Data Fig. 5c). Therefore, our results suggest that the ratio between the activity of the Go and NoGo neurons represents a probability that the presented stimulus belongs to either the Go or NoGo category.

Distortion of the orientation space underpinning categorization

In a previous study, we had shown that distortions of the orientation space could result from a modification of the neurons' excitability [29]. Therefore, we estimated the neuronal excitability in the orientation space by measuring the amplitude of the tuning curves of all the oriented V1 neurons (Fig. 5a). Neurons tuned to 45 ± 7.5° and 90 ± 7.5° had a similar peak amplitude (mean ± s.e.m, respectively 1.8 ± 0.2 and 1.5 ± 0.1 APrEs, permutation test p = 0.15, hedge's g for effect size = 0.12). However, neurons tuned for 67.5 ± 7.5° (at the location where the trough of activity separating the Go and NoGo domains) had a lower tuning curve amplitude (1.0 ± 0.1 APrEs; amplitude vs. 45° neurons' group: p=0.0001, g=0.43; amplitude vs. 90° neurons' group: p=0.0002, g = 0.41).

To assess continuously the amplitude of the tuning curves in the orientation space, we grouped the neurons in 7.5° bins, then plotted their mean tuning curve amplitude as a function of their orientation preference (Fig. 5b). For every Go/NoGo angle, we found the presence of a W-shaped distortion of the neuronal excitability in the orientation space. This distortion was characterized by two troughs of low excitability (mean location and 95% confidence interval: 68.3°, [66-70°] and 105.8°, [105-108°]; Fig. 5c) that corresponded to the flanks of the Go and NoGo orientations used during training separated

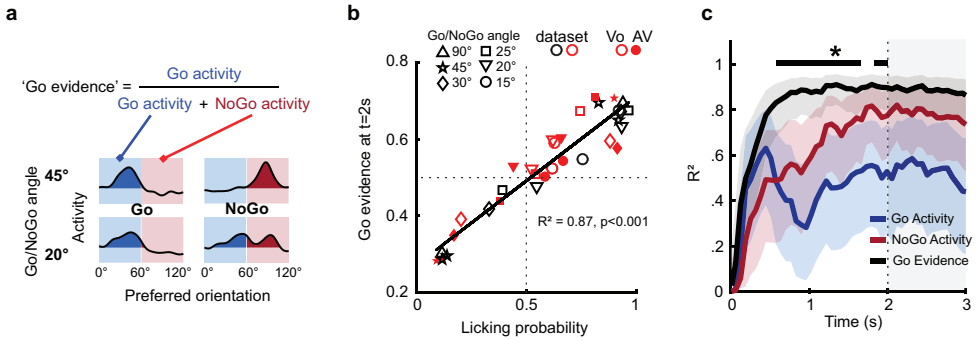

Fig. 4 | Categorical activity and behavioral performance. a. A boundary was set to separate the Go (1° - 60°) and NoGo (61° - 120°) domains of the orientation space. Go evidence is defined as the ratio between the amount of Go domain activity (area under the activation profile) and the sum of the Go and NoGo domain activity. **b.** Licking probability as a function of the Go evidence measured between 1,8 and 2 seconds after the beginning of the stimulus presentation for all the sessions of the two datasets. For the audiovisual dataset (red), we separated unimodal (empty symbols) and audiovisual (solid symbols) blocks. Black line: linear fit (r^2: 0.87; p<0.001). **c.** Value of the linear fit Pearson correlation coefficients as presented in (b) for all the timepoints of the visual stimulus presentation. Black line: Go evidence; blue line: Go domain activity; red line: NoGo domain activity. Shaded areas indicate the 95% confidence interval of the correlation coefficient. *: significant difference between Pearson correlation coefficient measured with the Go evidence and with the Go and NoGo activity (both values are outside of each other's confidence interval)

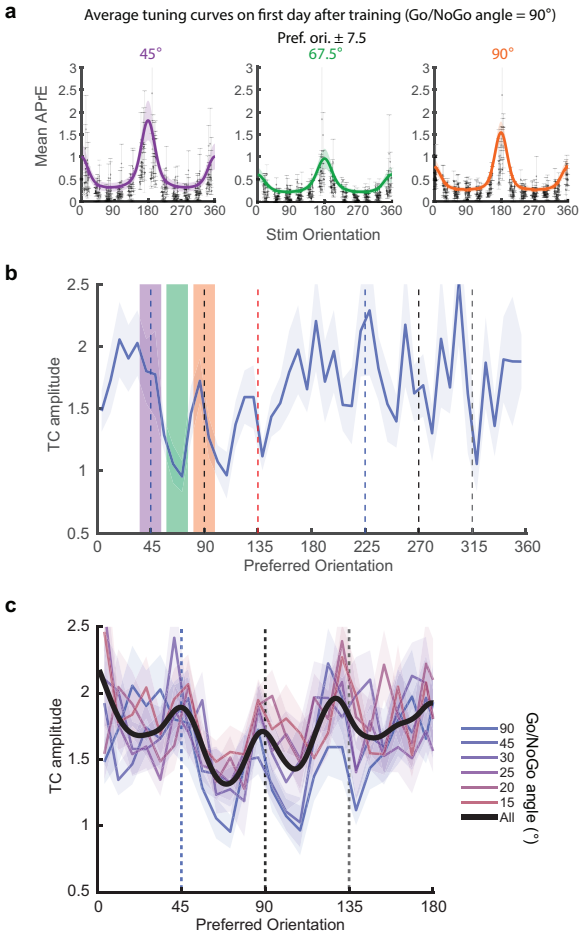

Fig. 5 | Modulation of the neuronal excitability in the orientation space. a. Tuning curves of the neurons tuned for 45 ± 7.5° (purple), 90 ± 7.5° (orange), and 67.5 ±7.5° (green), recorded during sessions when the Go/NoGo angle was 90°. **b.** Amplitude of the tuning curve as a function of the neurons' preferred orientation for the sessions when the Go/NoGo angle was 90°. **c.** Modulation of the neuronal excitability in the orientation space for the different Go/NoGo angles. Black trace: averaged modulation across Go/NoGo angles, fitted with a smoothing spline.

by a return to baseline excitability peaking at 88.3° (95% confidence interval: [86-91°]). We therefore tested the hypothesis that the W-shaped distortion of neuronal excitability in the orientation space could funnel the unbiased bottom-up neuronal activity toward the Go and NoGo domains. We qualitatively showed that the W-shaped distortion of the neuronal excitability in the orientation space can transform an orientation-unbiased input (a gaussian distribution of the neuronal activity centered in the orientation space on the orientation of the Go or the NoGo cue) into the experimental profiles obtained for all the Go/NoGo angles (Extended Data Fig. 6a,b). Moreover, as we had previously shown that pure tones sharpen orientation representations in the orientation space [34,35], we tested the effect of the W-shaped distortion of the neuronal excitability on sharper orientation inputs. We found that the resulting activity profiles evoked by the Go and NoGo cues at all Go/NoGo angles reproduced the experimental results obtained in the audiovisual block of our second dataset, i.e., a larger NoGo signal at the behavioral threshold in the presence of sound (Extended Data Fig. 6c). Altogether, this qualitative analysis suggests that the bimodal representation of the NoGo cues around the discrimination threshold can be supported by a simple multiplicative transformation of orientation unbiased responses by the W-shaped distortion of the neuronal excitability in the orientation space.

Discussion

The results presented in this study provide several important advances in our understanding of visual processing. First, we show that the similarity of neuronal representations in V1 i.e., the overlap in neuronal populations responding to two different stimuli, is a limiting factor for orientation discrimination. This could explain why decoding approaches based on extracting the differences between population responses are more successful than the animals' discrimination behavior [9]. Indeed, our results suggest that the entire population activity evoked by the visual stimulus in the relevant representational space is considered for the behavioral decision. Our second finding was unexpected as it goes against the dogma that the neuronal population in V1 encodes for the visual stimulus orientations [23]. Indeed, around the perceptual threshold, the representation of the NoGo cue in the orientation space was found to be bimodal with only a relatively weak activation of the neurons tuned for the NoGo stimulus orientation. Thus, in this specific behavioral context, V1 population does not encode for the stimulus orientation. The two distinct domains of the orientation space activated by the NoGo cue were composed of neurons tuned for the orientation of the Go visual stimulus (the Go domain) and neuronal population tuned for orientations located at equidistance between the orientations of the Go and the NoGo stimuli used during training (the NoGo domain). We first thought that the presence of those two domains of neuronal activity in the orientation space aimed at decreasing the overlap between the representation of the Go and NoGo cues. However, the large co-activation of the two orientation space domains for the presentation of the NoGo cue around the behavioral discrimination threshold ruled out this hypothesis. This also could explain why we found that similarity was not an accurate predictor of the mouse's behavioral choice. On another hand, the relative activity between those two domains of the orientation space was found to be a fine predictor of the animal's behavior. Interestingly, the information provided by V1 was found to be of a statistical nature. Indeed, erroneous choices could not be explained by V1 inaccuracies as the information present in V1 was similar in successful and unsuccessful trials. Therefore, the activity in V1 around the perceptual threshold seems to indicate an estimate by V1 of the probability that the visual stimulus is a Go cue or a NoGo cue. This finding is further supported by the demonstration that changing the relative activation of the Go and NoGo domain, by presenting the visual cues in an audiovisual context, results in a predictable improvement of the behavior. Hence, the animal decision is likely made by higher-order structures listening to those domains of the orientation space. This finding of a probabilistic encoding of the visual cue is in line with several theories of sensory processing, such as the hierarchical Bayesian inference hypothesis of visual processing 36. Altogether, our results supported by two independent datasets show that during an orientation task V1 does not encode for the orientations of the visual stimuli but provides a probabilistic classification of the stimulus in the Go and NoGo categories [12,37-39].

Finally, we found that the Go and NoGo domains are shaped by a distortion of the neuronal excitability in the orientation space. We had previously shown that learning can induce such distortions by generating a ring of low excitability around the task stimuli [29]. Therefore, it is likely that the W-shaped modulation of the neuronal excitability in the orientation space described in this study proceeds from the same mechanism. We also show, using a qualitative model, that the bimodal response in the orientation space can be explained by the multiplicative interaction between an evoked activity centered on the visual stimulus orientation with the modulation of the neuronal excitability in the orientation space. Future studies will be necessary to determine the cellular and network mechanisms underpinning this modulation of excitability and this transformation of the bottom-up neuronal activity.

References

1. Britten, K. H., Newsome, W. T., Shadlen, M. N., Celebrini, S. & Movshon, J. A. A relationship between behavioral choice and the visual responses of neurons in macaque MT. Vis Neurosci 13, 87–100 (1996).
2. Hung, C. P., Kreiman, G., Poggio, T. & DiCarlo, J. J. Fast readout of object identity from macaque inferior temporal cortex. Science 310, 863–6 (2005).
3. Salzman, C. D., Britten, K. H. & Newsome, W. T. Cortical microstimulation influences perceptual judgements of motion direction. Nature 346, 174–7 (1990).
4. Schiller, P. H. The effects of V4 and middle temporal (MT) area lesions on visual performance in the rhesus monkey. Vis Neurosci 10, 717–46 (1993).
5. Beck, J. M., Ma, W. J., Pitkow, X., Latham, P. E. & Pouget, A. Not noisy, just wrong: the role of suboptimal inference in behavioral variability. Neuron 74, 30–9 (2012).
6. Britten, K. H., Shadlen, M. N., Newsome, W. T. & Movshon, J. A. The analysis of visual motion: a comparison of neuronal and psychophysical performance. J Neurosci 12, 4745–65 (1992).
7. Chen, Y., Geisler, W. S. & Seidemann, E. Optimal decoding of correlated neural population responses in the primate visual cortex. Nat Neurosci 9, 1412–20 (2006).
8. Geisler, W. S. & Albrecht, D. G. Visual cortex neurons in monkeys and cats: detection, discrimination, and identification. Vis Neurosci 14, 897–919 (1997).
9. Stringer, C., Michaelos, M., Tsyboulski, D., Lindo, S. E. & Pachitariu, M. High-precision

coding in visual cortex. Cell 184, 2767-2778.e15 (2021).
10. Rumyantsev, O. I. et al. Fundamental bounds on the fidelity of sensory cortical coding. Nature 580, 100–105 (2020).
11. Petersen, R. S., Panzeri, S. & Diamond, M. E. Population coding in somatosensory cortex. Curr. Opin. Neurobiol. 12, 441–447 (2002).
12. Seidemann, E. & Geisler, W. S. Linking V1 Activity to Behavior. Annu. Rev. Vis. Sci. 4, 287–310 (2018).
13. Barlow, H. B. Single units and sensation: a neuron doctrine for perceptual psychology? Perception 1, 371–94 (1972).
14. Houweling, A. R. & Brecht, M. Behavioural report of single neuron stimulation in somatosensory cortex. Nature 451, 65–8 (2008).
15. Panzeri, S., Petroni, F., Petersen, R. S. & Diamond, M. E. Decoding neuronal population activity in rat somatosensory cortex: role of columnar organization. Cereb Cortex 13, 45–52 (2003).
16. Sriram, B., Li, L., Cruz-Martin, A. & Ghosh, A. A Sparse Probabilistic Code Underlies the Limits of Behavioral Discrimination. Cereb Cortex (2019) doi:10.1093/cercor/bhz147.
17. Wohrer, A. & Machens, C. K. On the number of neurons and time scale of integration underlying the formation of percepts in the brain. PLoS Comput Biol 11, e1004082 (2015).
18. Graf, A. B., Kohn, A., Jazayeri, M. & Movshon, J. A. Decoding the activity of neuronal populations in macaque primary visual cortex. Nat Neurosci 14, 239–45 (2011).
19. Seung, H. S. & Sompolinsky, H. Simple models for reading neuronal population codes. Proc Natl Acad Sci U A 90, 10749–53 (1993).
20. Shamir, M. Emerging principles of population coding: in search for the neural code. Curr Opin Neurobiol 25, 140–8 (2014).
21. Abdolrahmani, M., Lyamzin, D. R., Aoki, R. & Benucci, A. Cognitive modulation of interacting corollary discharges in the visual cortex. bioRxiv 615229 (2019) doi:10.1101/615229.
22. Lee, S. H. et al. Activation of specific interneurons improves V1 feature selectivity and visual perception. Nature 488, 379–83 (2012).
23. Hubel, D. H. & Wiesel, T. N. Receptive fields of single neurones in the cat's striate cortex. J Physiol 148, 574–91 (1959).
24. Priebe, N. J. Mechanisms of Orientation Selectivity in the Primary Visual Cortex. Annu. Rev. Vis. Sci. 2, 85–107 (2016).
25. Skottun, B. C. et al. Classifying simple and complex cells on the basis of response modulation. Vision Res. 31, 1079–1086 (1991).
26. Glickfeld, L. L., Histed, M. H. & Maunsell, J. H. Mouse primary visual cortex is used to detect both orientation and contrast changes. J Neurosci 33, 19416–22 (2013).
27. Poort, J. et al. Learning Enhances Sensory and Multiple Non-sensory Representations in Primary Visual Cortex. Neuron 86, 1478–90 (2015).
28. Resulaj, A., Ruediger, S., Olsen, S. R. & Scanziani, M. First spikes in visual cortex enable perceptual discrimination. Elife 7, (2018).
29. Corbo, J., McClure, J. P., Erkat, O. B. & Polack, P.-O. Dynamic distortion of orientation representation after learning in the mouse primary visual cortex. J. Neurosci. (2022).
30. Deneux, T. et al. Accurate spike estimation from noisy calcium signals for ultrafast three-dimensional imaging of large neuronal populations in vivo. Nat. Commun. 7, 12190 (2016).
31. Leo, F., Romei, V., Freeman, E., Ladavas, E. & Driver, J. Looming sounds enhance orientation sensitivity for visual stimuli on the same side as such sounds. Exp. Brain Res. 213, 193–201 (2011).
32. Romei, V., Murray, M. M., Cappe, C. & Thut, G. Preperceptual and Stimulus-Selective Enhancement of Low-Level Human Visual Cortex Excitability by Sounds. Curr. Biol. 19, 1799–1805 (2009).
33. McClure, J. P., Erkat, O. B., Corbo, J. & Polack, P.-O. Estimating How Sounds Modulate Orientation Representation in the Primary Visual Cortex Using Shallow Neural Networks. Front. Syst. Neurosci. 16, (2022).
34. McClure, J. P. & Polack, P.-O. Pure tones modulate the representation of orientation and direction in the primary visual cortex. J. Neurophysiol. 121, 2202–2214 (2019).
35. Ibrahim, L. A. et al. Cross-Modality Sharpening of Visual Cortical Processing through Layer-1-Mediated Inhibition and Disinhibition. Neuron 89, 1031–1045 (2016).
36. Lee, T. S. & Mumford, D. Hierarchical Bayesian inference in the visual cortex. J. Opt. Soc. Am. A 20, 1434 (2003).
37. Gilbert, C. D. & Li, W. Top-down influences on visual processing. Nat Rev Neurosci 14, 350–63 (2013).
38. Keller, G. B., Bonhoeffer, T. & Hubener, M. Sensorimotor mismatch signals in primary visual cortex of the behaving mouse. Neuron 74, 809–15 (2012).
39. Roelfsema, P. R. & Lange, F. P. de. Early Visual Cortex as a Multiscale Cognitive Blackboard. Annu. Rev. Vis. Sci. 2, 131–151 (2016).
40. Brainard, D. H. The Psychophysics Toolbox. Spat Vis 10, 433–6 (1997).
41. Pachitariu, M. et al. Suite2p: beyond 10,000 neurons with standard two-photon microscopy. 061507 (2017) bioRxiv doi:10.1101/061507.
42. Berens, P. et al. Community-based benchmarking improves spike rate inference from two-photon calcium imaging data. PLOS Comput. Biol. 14, e1006157 (2018).
43. Cronin, B., Stevenson, I. H., Sur, M. & Kording, K. P. Hierarchical Bayesian modeling and Markov chain Monte Carlo sampling for tuning-curve analysis. J Neurophysiol 103, 591–602 (2010).
44. Hentschke, H. & Stuttgen, M. C. Computation of measures of effect size for neuroscience data sets. Eur J Neurosci 34, 1887–94 (2011).
45. Fasano, G. & Franceschini, A. A multidimensional version of the Kolmogorov–Smirnov test. Mon. Not. R. Astron. Soc. 225, 155–170 (1987).

Methods

All the procedures described below have been approved by the Institutional Animal Care and Use Committee of Rutgers University, in agreement with the Guide for the Care and Use of Laboratory Animals.

Surgery

Ten minutes after systemic injection of an analgesic (carprofen, 5 mg per kg of body weight), adult (3-6 months old) male and female mice (first dataset: C57BL6; Jackson Laboratories # 000664), and for second dataset with unimodal visual and audiovisual conditions Gad2-IRES-Cre (Jackson Laboratories # 019022) × Ai9 (Jackson Laboratories # 007909) mice were anesthetized with isoflurane (5% induction, 1.2% maintenance) and placed in a stereotaxic frame. Body temperature was kept at 37°C using a feedback-controlled heating pad. Pressure points and incision sites were injected with lidocaine (2%). Eyes were protected from desiccation with artificial tear ointment (Dechra). Next, the skin covering the skull was incised, and a custom-made lightweight metal head-bar was glued to the skull using Vetbond (3M). In addition, a large recording chamber capable of retaining the water necessary for using a water-immersion objective was built using dental cement (Ortho-Jet, Lang). A circular craniotomy (diameter = 3 mm) was performed above V1. The AAV vector AAV1.eSyn.GCaMP6f.WPRE.SV40 (UPenn Vector Core) carrying the gene of the fluorescent calcium sensor GCaMP6f was injected in three sites separated by 500 µm around the center of V1 (stereotaxic coordinates: -4.0 mm AP, +2.2 mm ML from bregma) using a MicroSyringe Pump Controller Micro 4 (World Precision Instruments, WPI) at a rate of 30 nl/min. Injections started at a depth of 550 µm below the pial surface and the tip of the pipette was raised in steps of 100 µm during the injection, up to a depth of 200 µm below the dura surface. The total volume injected across all depths was 0.7 µl. After removal of the injection pipette, a 3-mm-diameter coverslip was placed over the dura, such that the coverslip fits entirely in the craniotomy and was flush with the skull surface. The coverslip was kept in place using Vetbond and dental cement. During the 5 days following surgery, mice were provided amoxicillin administered in drinking water (0.25 mg/mL). Mice were left to recover from the surgery for at least 3 weeks to obtain a satisfactory gene expression.

Behavioral training

Mice were water-deprived to 90% of their body weight and acclimated to head fixation on a spherical treadmill in custom-built, soundproof training rig. The rig was equipped with a monitor (Dell) and a water dispenser with a custom infrared beam lickometer. Data acquisition boards (National Instruments and Arduino) were used to actuate the solenoids for water delivery and vacuum reward retrieval, as well as recording the animal licking activity. The monitor and data acquisition boards were connected to a computer that ran a custom-made training program scripted in MATLAB. Once animals reached their target weight and were acclimated to the training setup, they were trained to perform the orientation discrimination task (Fig. 1A). In this task, drifting sine-wave gratings oriented 45° below the horizontal were paired with a water reward, and the animal was expected to lick (Go trial). Drifting gratings orthogonal to the Go signal (orientation 135°) signaled the absence of reward, and the animal was expected to withhold licking during those trials (No-Go trial). The Go and NoGo cues had the same temporal frequency (2 Hz), spatial frequency (0.04 cycle per degree), duration (3 seconds) and contrast (75%). When the stimulus instructed the animal to lick, the water delivery had to be triggered by the mouse licking during the third second of the stimulus presentation. No water was dispensed in the no-lick condition or if the mouse failed to trigger water delivery in the lick condition. If the animal responded correctly (Hit or Correct Rejection), the intertrial interval was 3 s. If the animal responded incorrectly (Miss or False Alarm), the intertrial interval was increased to 6 s as a negative reinforcement (Fig. 1A). Performance was measured using the D' statistic (D'=norminv(Hit rate) - norminv(False alarm rate), norminv = inverse of the normal cumulative distribution function). Animals were considered experts if their performance during training sessions was greater than 1.7.

Best random D'. Our training strategy was that mice first acquired a strongly reliable licking behavior for the Go, then learned to withhold from licking in NoGo trials. Hence, the improvement of their performance during training was primarily driven by decrease in the False Alarm rate. To take into account the constant bias of mice toward licking, we computed the best random D' value using a probability of licking in response to the Go cue that corresponded to the average Hit rate over the six recording sessions. The best random D' was defined as the point where the mouse would differentiate the NoGo cue from the Go cue in half of the trials, i.e., a FA rate of 50%. For the first dataset, we therefore considered a binomial distribution of p=0.93 and n=128

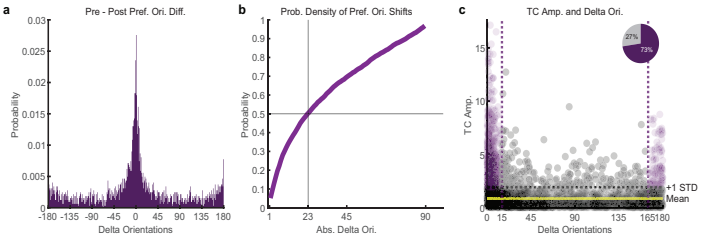

Extended Data Fig. 1 | V1 neurons' preferred orientations estimated at the beginning and at the end of the recording session. a. Distribution probability of the shift in orientation preference (delta orientation) estimated before (pre) and after the behavioral task (post; n = 3 mice). Tuning curves were generated using the neurons' activity evoked by the grifting gratings presented during a tuning block (10 trials for each of the 12 orientations). The distribution is centered onto 0. **b.** Probability distribution of the absolute value of the orientation shift (Abs. Delta Ori.). 50% of the neurons with an orientation preference had a shift of less than 23° (median shift). **c.** Amplitude of the response of the neurons for their preferred orientation (TC amp.: tuning curve amplitude) as a function of the shift in orientation preference. To determine the neurons most likely to participate in the representation of the task stimuli, we computed the mean and standard deviation (SD) of the tuning curve amplitude of neurons with the largest shifts (15° to 165°). The activity threshold was defined as the mean + 1SD. 73% of the neurons with a tuning curve amplitude greater than this threshold had a preferred orientation shift of less than 15° (purple neurons).

(average number of trials) for the Go behavior, and of p=0.5 and n=128 for the NoGo behavior. We used the 77.5 and 22.5 percentiles to simulate the best hit rate and FA rate that could be obtained (p=0.05) given these underlying probabilities. This led to a value of D' = 1.68. For the second dataset, where animals licked less for the Go when the Go/NoGo and the number of trials was lower, we used a binomial distribution of p=0.77 and n=60 for the Go and p=0.5 and n=60 for the NoGo, yielding a value of D' = 1.0. These values correspond to the D' values above which we can conclude that mice do not behave at random for the NoGo trials, not to the perceptual threshold.

Imaging sessions.
First dataset (unimodal visual trials only). Calcium imaging in V1 was performed over 6 consecutive days. During those sessions, the orientation of the Go signal remained at 45°, while the orientation of the NoGo signal was set to 135° for the first session, 90° for the second, 75° for the third, 70° for the fourth, 65° for the fifth, and 60° for the sixth. Hence the angle between the Go and the NoGo cues was progressively decreased: Day 1: 90°, Day 2: 45°, Day 3: 30°, Day 4: 25°, Day 5: 20° and Day 6: 15° (Fig. 1A). Our decision to generate a psychometric curve and a neurometric curve over six consecutive days was motivated by the following reasons. [1] We needed the mouse behavior to be driven by the perceptual difficulty not the task difficulty. Our goal was therefore to make sure that mice continuously understood the task they were trained for. By decreasing gradually, the angle between the Go and NoGo cue we made sure that the mouse fully understood the task rules. The mice result in being better trained for the latest sessions (e.g., when the Go/NoGo angle is 15°) than for the earliest sessions (e.g., when the Go/NoGo angle is 45°). However, this is unlikely to affect the conclusion we can draw from our experiments. [2] The Go signal was also kept constant across sessions to simplify the task rules for the mouse and allow for a better estimate of the mouse orientation discrimination threshold (decreasing the chance that the animal does not perform because it does not understand the task rules). Moreover, this decreased the number of free parameters in our experiments, as the NoGo orientation is the only parameter that changes across the completion of the task. [3] Finally, as V1 activity is very sparse and highly variable from trial to trial, we also wanted to work with a large number of trials for each Go/NoGo angle. Mice typically perform a maximum of 200 trials per training session. However, to make sure that mice were optimally motivated to perform the task while we were recording, we kept the number of trials to 120 to avoid misses and correct rejection trials due to a lack of motivation to perform the task.

Second dataset (unimodal visual and audiovisual trials). In this dataset (generated by a different experimenter), calcium imaging in V1 was performed during 5 consecutive daily sessions using the same visual stimuli as described above for the first dataset starting from a Go/NoGo angle of 45°. The only difference was that the sessions were divided into 4 blocks of

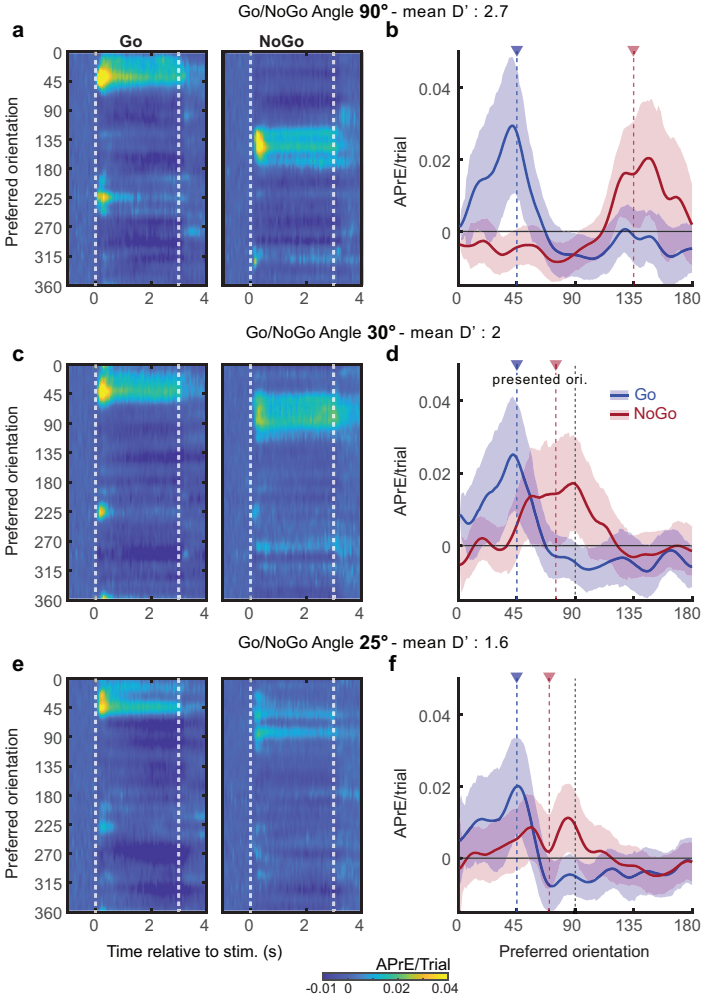

Extended Data Fig. 2 | Go and NoGo stimulus representations in the orientation space as a function of the Go/NoGo angle (first dataset, unimodal visual). a. Neuronal activity evoked by the Go (left panel) and NoGo stimuli (right panel) as a function of V1 neurons' preferred orientations when the Go/NoGo angle is 90°. Neuronal activity color scale is located at the bottom of the (e) panel. The mean behavioral performance (D') across mice is indicated on top. **b.** Mean activity evoked in the orientation space by the Go (45°, blue) and NoGo (135°, red) stimuli during the two first seconds of the stimulus presentation. Vertical colored lines indicate the orientation of the presented stimulus. Shaded areas indicate the s.e.m. **c.** Same representation as in (a) when the angle between the Go/NoGo angle is 30°. **d.** Same representation as in (b) when the NoGo orientation is 75°. **e.** Same representation as in (a) when the Go/NoGo angle is 25°. **f.** Same representation as in (b) when the NoGo orientation is 70°.

30 trials alternating unimodal visual and audiovisual blocks (see below; Fig 3A) At the beginning of the recording session, the first block was randomly selected between unimodal visual and audiovisual.

Recording sessions. Recordings were made of three types of blocks: unimodal visual, audiovisual (only for the second dataset), and tuning blocks. For all those blocks, the gratings had the same temporal frequency (2 Hz) and spatial frequency (0.04 cycle per degree). The duration was 3 seconds for the unimodal visual and audiovisual blocks and 1.5s in the tuning blocks. The contrast of the drifting gratings was 25% during testing (compared to 75% during training) to enhance the impact of sounds on representation of the visual stimuli orientation in V1 (sound modulation in V1 was shown to follow the principle of inverse effectiveness 34,35). Auditory stimuli during the audiovisual blocks consisted of the presentation of one of two sinewave pure tones (10 kHz and 5 kHz; 78 dB; duration: 3 seconds). Sounds were produced by a speaker located immediately below the center of the screen. Visual and auditory stimuli were generated in Matlab (MathWorks) using the Psychtoolbox 40. The background noise (room heat and air conditioning

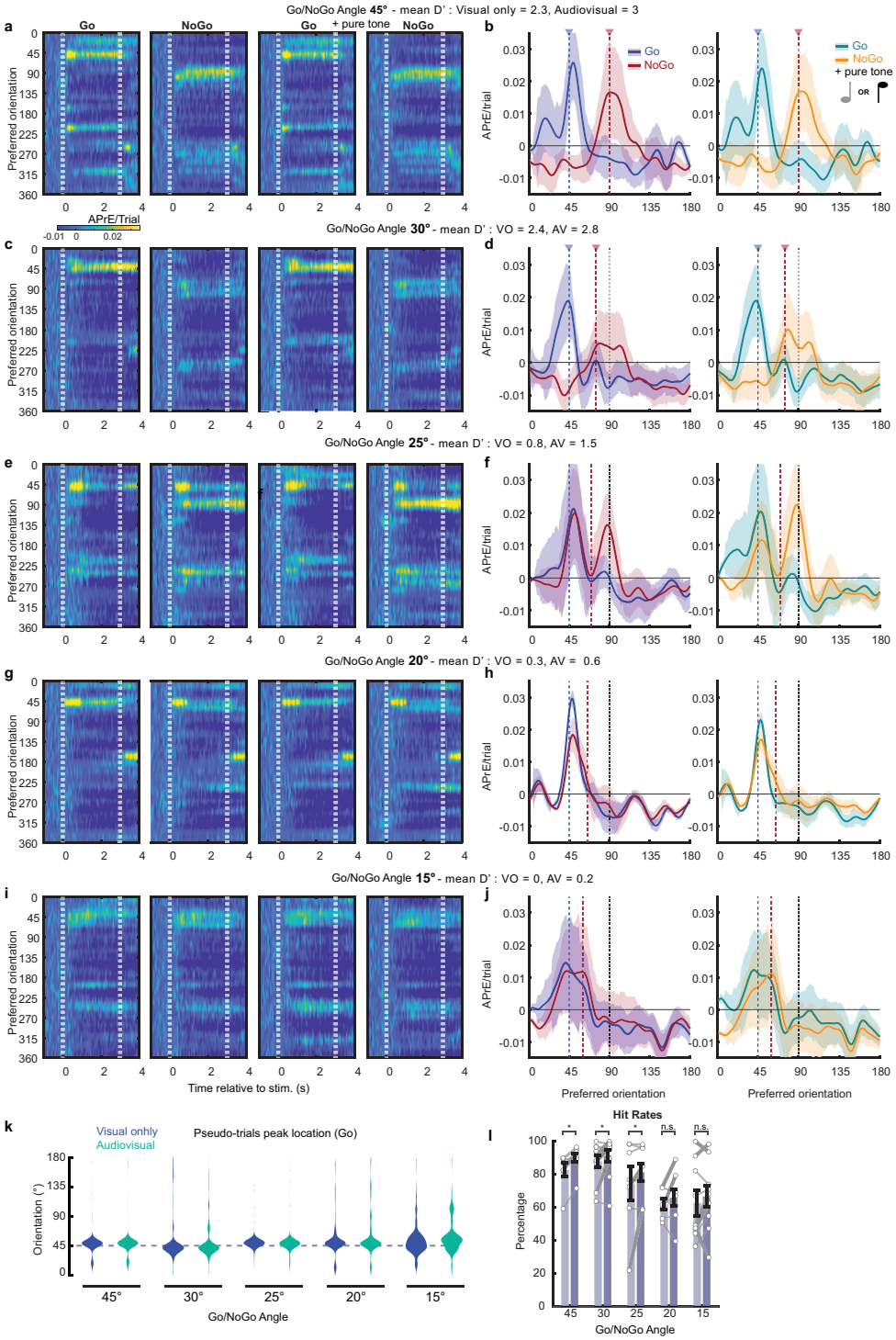

Extended Data Fig. 3 | Go and NoGo stimulus representations in the orientation space as a function of the Go/NoGo angle (second dataset: unimodal visual and audiovisual blocks). a. Neuronal activity evoked by the Go (first panel on the left) and NoGo stimuli (second panel on the left) as a function of V1 neurons' preferred orientations when the Go/NoGo angle is 45° in the unimodal visual blocks. Right panels: same representation for the Go (third panel) and NoGo stimuli (fourth panel) presented in the audiovisual blocks. Neuronal activity color scale is located at the bottom of the panel. The mean behavioral performance (D') across mice is indicated on top. **b.** Left panel: mean activity evoked in the orientation space by the Go (45°, blue) and NoGo (90°, red) stimuli during the two first seconds of the stimulus presentation in the unimodal visual blocks. Right panel: mean activity evoked in the orientation space by the Go (45°, cyan) and NoGo (90°, orange) stimuli during the two first seconds of the stimulus presentation in the audiovisual blocks. Vertical colored lines indicate the orientation of the presented stimulus. Shaded areas indicate the s.e.m. **c.** Same representation as in (a) when the angle between the Go/NoGo angle is 30°. **d.** Same representation as in (b) when the NoGo orientation is 75°. **e.** Same representation as in (a) when the Go/NoGo angle is 25°. **f.** Same representation as in (b) when the NoGo orientation is 70°. **g.** Same representation as in (a) when the Go/NoGo angle is 20°. **h.** Same representation as in (b) when the NoGo orientation is 65°. **i.** Same representation as in (a) when the Go/NoGo angle is 15°. **j.** Same representation as in (b) when the NoGo orientation is 60°. **k.** Violin plot of the distribution of the location in the orientation space of the peak of activity for unimodal Go (blue) and audiovisual Go (cyan) pseudo-trials. Dotted line indicates the orientation of the presented Go stimulus. **l.** Hit rates during the unimodal visual (light purple) and audiovisual (dark purple) blocks of the recording session for the different Go/NoGo angles. Black lines indicate mean ± s.e.m. across sessions. Statistic test: ns: p>0.05; *: p<0.05; ***: p<0.001. White dots indicate individual mice (thick lines indicate significant difference; p<0.05).

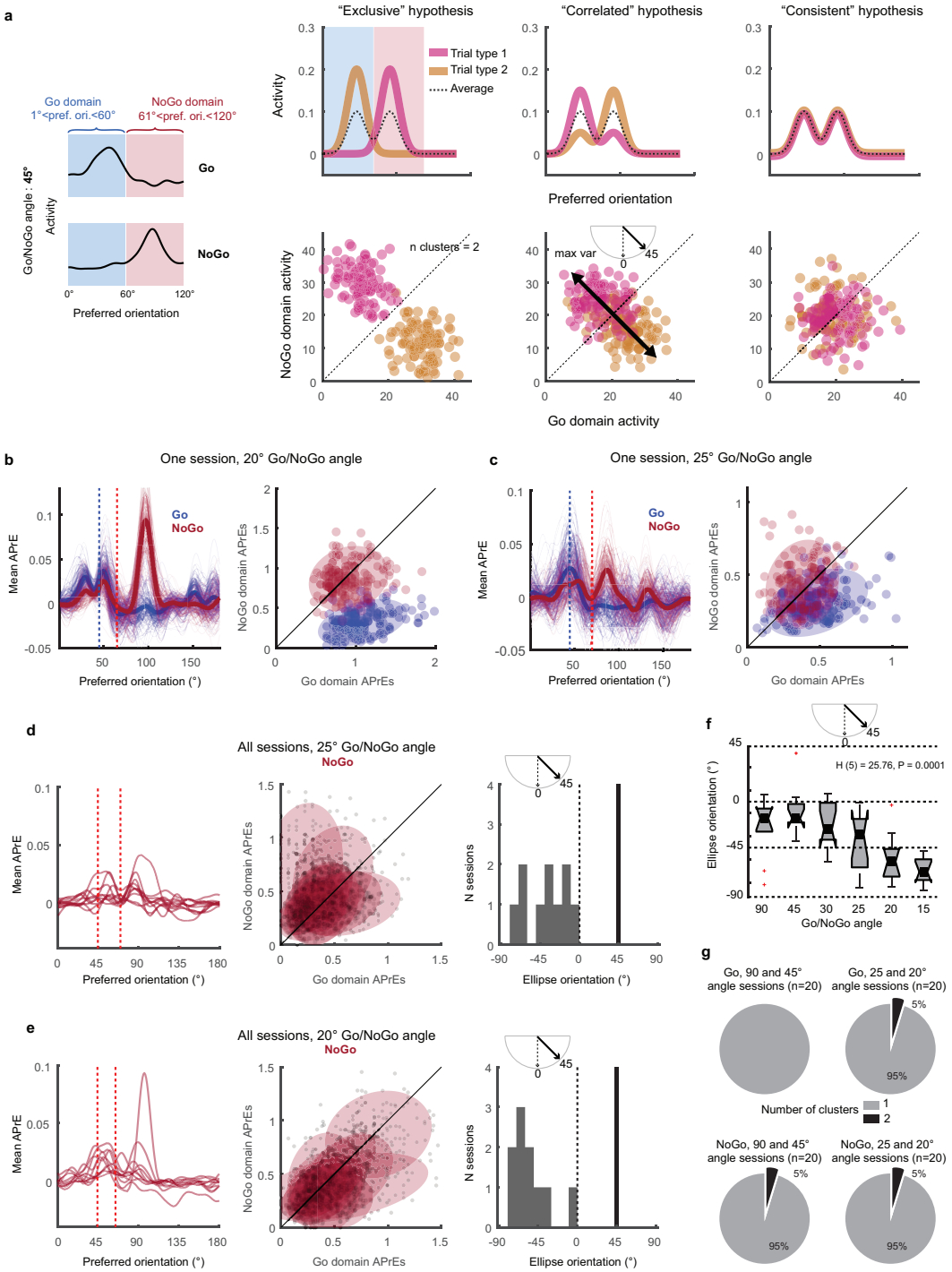

Extended Data Fig. 4 | Bimodal NoGo representations during single trials. a. Schematic description of the tested hypotheses. The bimodal representations of the NoGo cue for Go/NoGo angles between 20° and 30° found by averaging across trials (black dotted lines) could result from: (i) the activation of the neurons tuned for the Go orientation (Go domain; gold) and neurons tuned for the NoGo orientation or the NoGo attractor (NoGo domain; magenta) in different trials ("exclusive hypothesis", top left panel) - in which case, plotting the relative activity in the Go domain and NoGo domain for each trial would lead to a plot with two distinct clusters (bottom left panel), (ii) the simultaneous activation of the Go and NoGo domain in each single trials ("consistent hypothesis": top right panel) – in which case the Go and NoGo domain are similarly activated across trials leading to a single cluster (bottom right panel). Finally, an intermediate hypothesis, where for each trial the activation of Go domain is anti-correlated to the activation of NoGo domain ("correlated hypothesis": top center panel) which would lead to a single cluster elongated along an axis perpendicular to the line of equity (axis angle: 45°; see inset of bottom center panel). **b.** Example of one session of the first dataset during which the Go/NoGo angle was 20°. Note that both the Go and NoGo trials are represented by a single cluster. The Go stimulus mostly activate the Go domain while the NoGo cues activate similarly Go and NoGo domains (cluster on the line of equity). **c.** Example of one session during which the Go/NoGo angle was 25°. Note the similarity of those results with those presented in (b). **d.** Response profiles across the 2 first second of the stimulus presentation (left panel) for all the sessions of the first dataset when the Go/NoGo angle was 20°. Those profiles lead to single clusters (central panel) which maximum variance axis is ranges between 0° and -90° (right panel), disproving the exclusive and anti-correlated hypotheses. **e.** Same representation as in (d) for the all the sessions of the second dataset when the Go/NoGo angle was 25°. **f.** Distribution of the maximal variance orientation for all the Go/NoGo angles disproving the "anti-correlated hypothesis". Kruskal Wallis: $H(5)=25.76$; $p = 0.0001$. **g.** In most sessions, neuronal activity evoked by the Go (top panels) and NoGo (bottom panels) single trials generate a single cluster (optimal number of cluster evaluated with the Calinski-Harabasz criterion) in the Go/NoGo domains activation space, disproving the "exclusive hypothesis". Altogether, those analyses prove that the NoGo and Go domains are co-activated by the NoGo stimuli at the single trial level when the Go/NoGo angle is near the limit of perceptual discrimination.

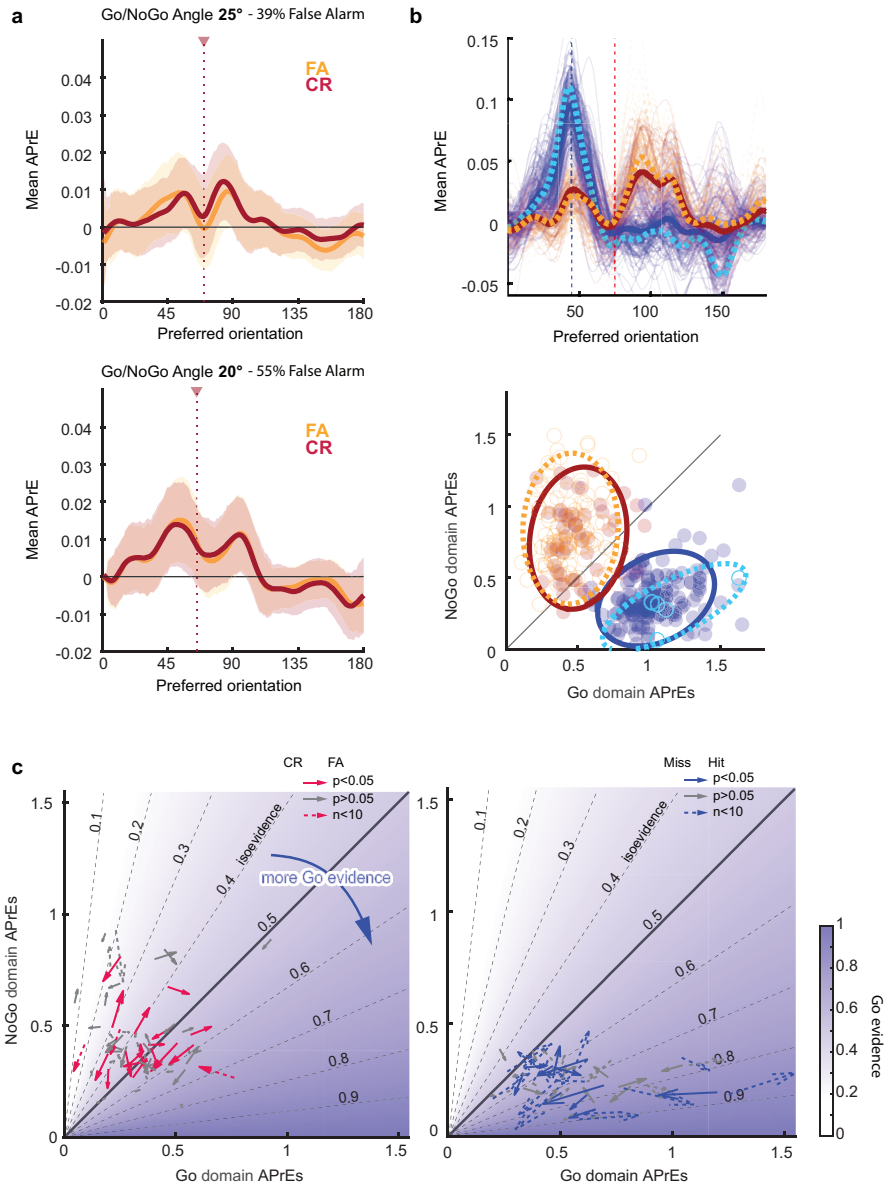

Extended Data Fig. 5 | False alarm trials are not explained by largest evidence for the Go in V1. a. Activation profiles in the orientation space evoked by the NoGo cue in V1 for False Alarms (FA, yellow) and Correct Rejection (CR, red) in the first dataset (top panel; Go/NoGo angle = 25°, bottom panel; Go/NoGo angle = 20°). **b.** Activation profile (left panel) and Go/NoGo activation diagram (right panel) for all the trials of one recording session of the first dataset (Go/NoGo angle = 45°) when separating FA (yellow), CR (red), Hit (blue) and Miss (cyan) trials. **c.** Arrows representing the translation of the clouds of single trials Go/NoGo activation between CR and FA (left) and Misses and Hits (right). Grey arrows indicate non-significant translations (two-dimension Kolmogorov-Smirnoff test). Dotted lines indicate sessions for which there was less than 10 trials with one of the trial types. Most translations follow the line of isoevidence (i.e., Go activation / (Go activation + NoGo activation) = constant)

airflow, laser cooling fans, and spherical treadmill airflow) was 69 dBA. Each audiovisual trial resulted from the random combination of one of the two pure tones with one of the two drifting gratings of the session. For each imaging session, we assessed the orientation tuning of the imaged neurons in an orientation tuning block that consisted in the presentation of a series of drifting sinewave gratings (12 orientations evenly spaced by 30 degrees and randomly permuted). The tuning block was usually located at the end of the imaging session. However, placing the tuning block at the beginning of the recording session did not change our estimation of the neurons preferred orientation (Extended data Fig. 1). The spatiotemporal parameters of tuning block stimuli were identical to those of the behavioral block except for their duration and contrast (temporal frequency = 2 Hz, spatial frequency = 0.04 cycle per degree, contrast = 100%; duration: 1.5 seconds; intertrial interval: 3 seconds). As scanning was not synchronized with the stimulus presentation, a photodiode located at the top left corner of the screen was used to detect the exact timing of the visual stimuli onset and offset. The photodiode signal was acquired along with the following signals: 1) a signal provided by the two-photon microscope, which indicated the onset of each frame, and 2) two analog signals encoding the orientation of the drifting grating and the frequency of the auditory stimulus. These signals were digitized (NiDAQ, National Instruments) and recorded with the software WinEDR (John Dempster, University of Strathclyde). Ball motion was tracked by an IR camera taking pictures of the ball at 30 Hz. Eye motion was monitored at 15 Hz using a second IR camera imaging the reflection of the eye on an infrared dichroic mirror. Functional imaging was performed at 15 frames per second using a resonant scanning two-photon microscope (Neurolabware) powered by a Ti-Sapphire Ultra-2 laser (Coherent) set at 910 nm. The scanning mirrors of the Neurolabware microscope are in a hermetically sealed chamber, bringing the scanning hum below the room ambient noise (< 59 dBA). The laser beam was focused 200 microns below the cortical surface using a 16×, 0.8 NA Nikon water-immersion objective. The objective was tilted 30 degrees such that the objective lens was parallel to the dura surface. Laser power was kept below 70 mW. Frames (512x796 pixels) were acquired using the software Scanbox developed by Neurolabware.

Data analysis

Imaging data pre-processing. Calcium imaging frames were realigned offline to remove movement artifacts using the Scanbox algorithm (Neurolabware). For the first dataset (see Table 1), a region of interest (ROI) was determined for each neuron using an automatic segmentation and pre-processing routine (Suite2P[41]). The second dataset (see Table 1) was segmented by hand. For every frame, the fluorescence level was averaged across the pixels of the ROI. Potential contamination of the soma fluorescence by the local neuropil was removed by subtracting the mean fluorescence of a 2-5-micron ring surrounding the neuron's ROI, excluding the soma of neighboring neurons, and then adding the median value across time of the subtracted background. We then computed the fractional fluorescence from the background subtracted fluorescence data. The fractional fluorescence ($dF/F = (F - F_0) / F_0$), was calculated with F_0 defined as the median of the raw fluorescence measured during every inter-trial interval, then was deconvolved into Action Potential related Events (APrEs) using a benchmarked deconvolution algorithm [30,42]. Only neurons whose correlation between the inferred fractional fluorescence (convolved back from the inferred AprEs) and the measured fractional fluorescence was greater than 0.8 were used for the analysis. This inclusion criterion removed neurons for which the calcium signal was too poor to allow the algorithm to accurately detect AprEs. Additional inclusion criteria were used for the automatically segmented dataset ('iscell' variable from Suite2P > 0.8, minimum area > 15 μm^2, roundness (% of overlap with a circle centered on the ROI) > 20, and response probability for the preferred orientation of the Tuning Block >0.1). Trials were isolated and stored on a SQL database.

Tuning curves. The orientation tuning curve of each neuron was fitted to the APrE responses recorded during the tuning curve blocks using a Markov chain Monte Carlo sampling-based Bayesian method [29,34,43] based on a Poisson noise model. This algorithm fitted 4 different models to the observed responses ("circular gaussian 360°" for orientation but not direction selective tuning curves, "circular gaussian 180°" for strictly direction selective tuning curves, "direction selective circular gaussian" for direction and orientation tuned neurons, and "constant" for untuned neurons). The fit that explained best the data was then selected. If the constant model was the best fit, the

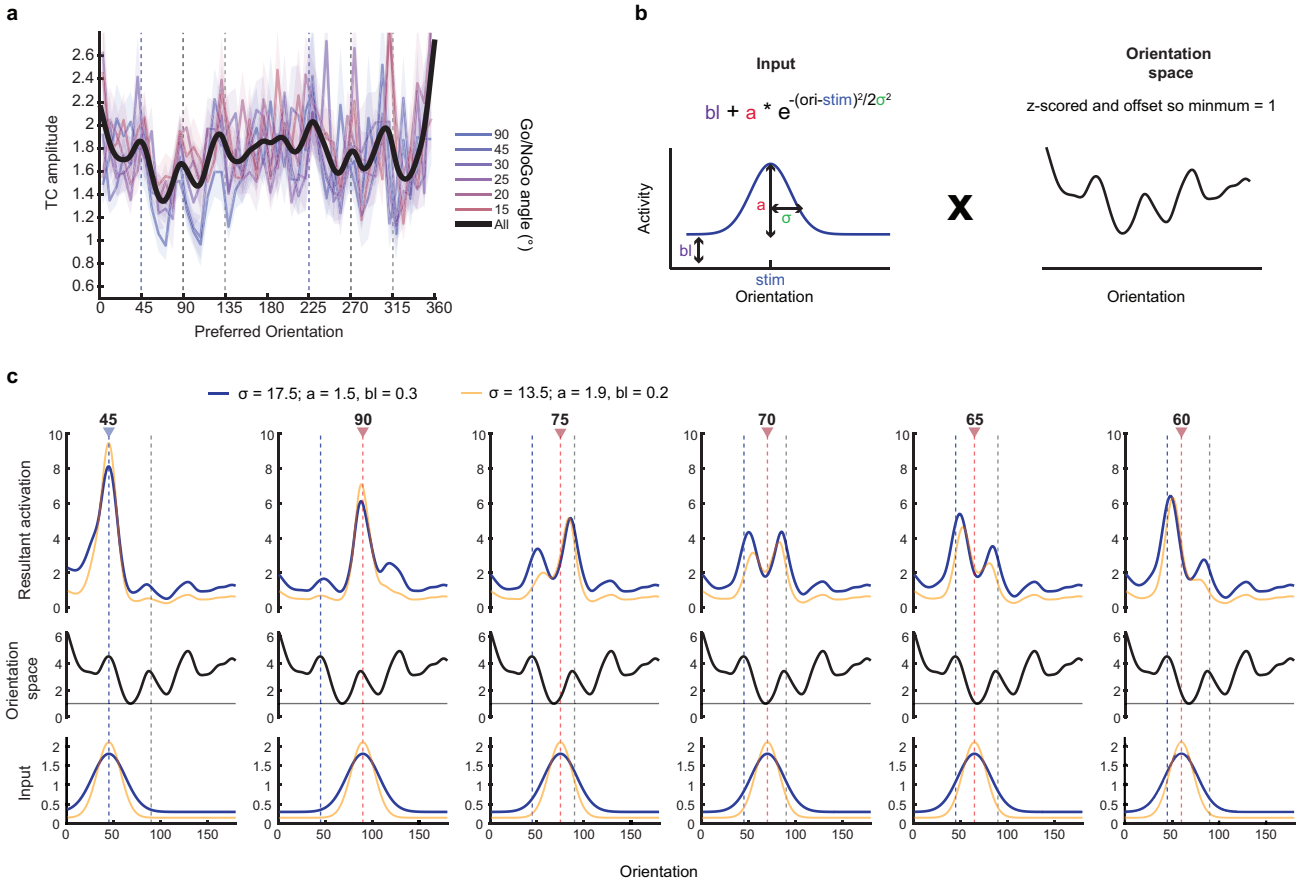

Extended Data Fig. 6 | Putative mechanism underpinning the bimodal representation of the NoGo cues in the orientation space. a. Modulation of the neuronal excitability in the orientation space (0-360°) for the different Go-NoGo angles. Black trace: averaged modulation across sessions. A modulation of the neuronal excitability in the orientation space is also found for neurons preferring gratings drifting in the opposite direction. **b.** Testing the effect of a multiplicative interaction between a unimodal activation in the orientation space by the visual stimulus (modelling a 'pure' bottom input to layer 2/3; left panel) and the modulation of the neuronal excitability in the orientation space found experimentally in layer 2/3 (right panel). **c.** Effect (top panels) of the multiplicative interaction between a unimodal visual activation of the orientation space (bottom panels) and the modulation of the neuronal excitability in the orientation space (middle panel) for each Go/NoGo angle (columns). Vertical lines indicate the orientation of the presented stimulus (blue: Go orientation, purple: NoGo orientations). Blue traces: inputs and outputs corresponding to the presentation of the stimulus in the unimodal visual context. Yellow traces: inputs and outputs corresponding to the presentation of the stimulus in the audiovisual context. The effect of sound on the inputs (decrease of baseline, increase of peak and decrease of width) was qualitatively modeled after observations reported in Ibrahim et al., 2016. Those results qualitatively reproduce the activity profiles obtained experimentally.

neuron was considered not tuned. The preferred orientation was defined as the peak of the fitted orientation tuning curve. When a neuron was not direction selective (i.e., responding equally to the same oriented stimulus moving in opposite directions), the preferred orientation was defined as the orientation included in the range [0 – 180]. Similarity. For each recording session, the mean evoked activity across time of the n simultaneously recorded neurons was represented by an n-dimensional vector. The similarity was obtained by computing the cosine of the angle between the vectors of evoked activity of Go and NoGo trials. The same procedure was then repeated using all recorded neurons. The point with the maximum deviation from the baseline value (mean similarity measured during the 1 second period immediately preceding the stimulus presentation) during the first second of the stimulus presentation was used to capture the relationship between similarity and performance.

Representation of the neuronal activity in the orientation space. To allow a full coverage of the orientation space, neurons were pooled across similar recording sessions (for a same Go/NoGo angle and a same dataset). The preferred orientation of every neuron was assessed (using the fits of the APrE responses recorded during the tuning block, see above). A subset of ROIs did not show significant orientation or direction tuning in first dataset without inclusion criteria (18.18%, n = 12602/69317). When the inclusion criteria (i.e., 'iscell' parameter from Suite2P, roundness, minimum area and response probability) were applied, all of the neurons showed a reliably estimated orientation or direction tuning. In the second dataset, a large subset of the segmented 'neurons' did not show significant orientation or direction tuning (46.89%, n = 1667/3555), and were excluded from further analysis. For each stimulus of each group (e.g., 45° presented to trained mice), we generated an orientation space activity map, sorting neurons according to their preferred orientation. Their activity was then averaged across trials, baseline-subtracted, and averaged across neurons sharing the same preferred orientation. To access the variability across trials of the pooled pseudo-population, we generated 1,000 resampled trials using the following procedure. For each resampled trial, 250 neurons (~15% of the neurons of the database) were randomly selected, and for each neuron, one trial from the test block during which the stimulus of interest was presented (e.g., 45°) was selected at random. The activity of the neuron during the selected trial was included in an orientation*time matrix in which rows corresponded to the neurons' preferred orientations (bin: 1°). The resulting trial matrix was baseline-subtracted and smoothed across the orientation space by a Gaussian weighted mean (std= 6°).

Locomotion and pupil size. We did not consider those parameters further in this study. We had already shown that arousal and locomotion could not account for those sound modulation of visual processing (McClure and Polack, 2019). We had also ruled out that arousal and locomotion could not account for the distortion of the orientation space found in mice trained to perform an orientation discrimination task (Corbo et al., 2022). Those results are in line with several studies that have recently demonstrated that the modulation of the V1 neuronal activity by behavioral parameters such as locomotion and arousal are orthogonal to orientation encoding (Hajnal et al., 2021; Stringer et al., 2021).

Mean tuning curves comparison. To compare the tuning curves of neurons in specific bins of orientation preference, the tuning curve fit of all considered neurons was circularly shifted so that the peak would be centered at 0°. To visualize the data underlying the averaged fits, the APrE responses were shifted by the same number of degrees. For example, the data from a neuron with a preferred orientation of 45° was shifted by -45° such that its response to 0° would show at -45° on the plot, its response to 30° would show at -15°, etc. The median of each individual neuron's responses was then computed, and for each degree of the orientation space the medians from all neurons falling in that degree (that were equally shifted) were averaged.

Excitability across orientation space. The amplitudes of the tuning curve fits of all neurons from sessions of the first dataset having the same Go/NoGo angle were sorted according to their preferred orientation (bin width = 7.5°) and averaged for each bin. The same operation was performed including all the neurons from all the sessions of the first dataset, and the result was fitted using a smoothing spline (MATLAB fit function, smoothing parameter = 0.01). Using different smoothing methods (rolling average, gaussian weighted rolling average) or bin sizes did not change the results(not shown). The mean location of the peak and troughs and their confidence intervals were obtained with bootstrapping the tuning curve amplitude data 1000 times, fitting the smoothing spline, and locating the local maxima and minima.

Statistics

To determine if the means of two distributions (amplitude of tuning curves, behavioral responses, and D') were significantly different, we compared the observed difference with the distribution of 10,000 differences obtained when the labels were shuffled. The two-tailed confidence interval of the null hypothesis at the alpha level 0.05 was defined as the 2.5 and 97.5 percentile of the distribution obtain from the permutations. The difference between the observed means was considered significant if located outside the confidence interval of the null distribution.

Because large number of observations can lead to conclude on significant differences of even irrelevantly small magnitude, we complimented relevant tests with an effect size measure, Hedges'g, using a MATLAB toolbox 44. Traditionally, values under 0.2 correspond to the absence of effect, values between 0.2 and 0.4 are considered to reflect a small effect, values between 0.4 and 0.6 correspond to a medium effect, and values larger than 0.6 correspond to a large effect size.

Supplementary Methods

Bimodality at the trial level. To assess whether the coactivation of the Go and NoGo domains observed in the average of the pseudo-population was present within an individual session and at the trial level, we analyzed the population activity of single trials in the Go/NoGo domains space. For every trial, the APrEs evoked during the two first seconds of stimulus presentation by all the neurons with preferred orientation ranging between 1° and 60° (Go domain) or 61° and 120° (NoGo domain) were summed and divided by the number of neurons considered. For each trial, we then plotted the activity measured in the Go domain versus the activity measured in the NoGo domain. An ellipse was fitted on that cloud so it would encompass 95% of the trials in that space. The orientation of the ellipse being aligned with the orientation of largest variance of the point cloud, it was used to compare the variance measured in every session to the expected variance orientation that would be observed if a Go/NoGo coactivation would not happen at the trial level. Additionally, the optimal number of clusters to explain the data was evaluated with the Calinski-Harabasz criterion (MATLAB evalclusters function).

V1 representation and decision at the trial level. To test whether the clouds of single trial activity in the Go/NoGo domains space were different when trials were split according to the behavioral decision of the animal, we used a two-dimension extension of the Kolmorogov-Smirnov test45. The direction of the of the cloud displacement between successful and unsuccessful trials was assessed by drawing a line between the centroid of the two clouds.

Data availability

All data are available from the corresponding author upon reasonable request.

Acknowledgements

This work was funded by the Whitehall Foundation (grant 2015-08-69), the Charles and Johanna Busch Biomedical Grant Program, and the National Institutes of Health (National Eye Institute: Grant #R01 EY030860; Brain initiative: Grant #R01 NS120289). J.C. was supported by a Fyssen Foundation postdoctoral fellowship. The authors are grateful to the members of the laboratory for their comments on the manuscript.

Author Contributions

B.E. performed the experiments to generate the unimodal visual dataset; J.M. performed the experiments to generate the audiovisual dataset; H.K. demonstrated the feasibility of the effect of sounds on mouse visual discrimination threshold; J.C. designed and performed the analysis with contributions from P-O.P. B.E., and J.M.; P-O.P. designed and supervised the study with contributions from J.C; J.C. and P-O.P. wrote the manuscript with feedbacks from all the co-authors.

Competing interests.

The authors declare no competing financial interests.